Eur. Phys. J. C 21, 291–301 (2001)
Digital Object Identifier (DOI) 10.1007/s100520100736

THE EUROPEAN PHYSICAL JOURNAL C

Radiative four-fermion processes at LEP2

G. Montagna[1], M. Moretti[2], O. Nicrosini[1], M. Osmo[1], F. Piccinini[1]

[1] Dipartimento di Fisica Nucleare e Teorica, Università di Pavia and INFN, Sezione di Pavia, via A. Bassi 6, 27100 Pavia, Italy
[2] Dipartimento di Fisica, Università di Ferrara and INFN, Sezione di Ferrara, Ferrara, Italy

Received: 14 March 2001 / Revised version: 26 June 2001 /
Published online: 3 August 2001 –

Abstract. The production of four fermions plus a visible photon in electron–positron collisions is analyzed, with particular emphasis on the LEP2 energy range. The study is based on the calculation of exact matrix elements, including the effect of fermion masses. In the light of the present measurements performed at LEP, triple and quartic anomalous gauge couplings are taken into account. Due to the presence of a visible photon in the final state, particular attention is paid to the treatment of higher-order QED corrections. Explicit results for integrated cross sections and differential distributions are shown and commented on. The features of the Monte Carlo program WRAP, used to perform the calculation and available for experimental analysis, are described.

1 Introduction

One of the main goals of electroweak physics at LEP2 is the study of the properties of the W bosons [1]. The center of mass (c.m.) energy above the threshold of W pair production offers the possibility to extract information about the mass and couplings of the W boson from the analysis of four-fermion ($4f$) final states. As is well known, because of the precision of the experimental measurements, radiative corrections to $e^+e^- \to 4f$ processes are needed in order to provide suitable theoretical predictions [1,2]. From this point of view, events with four fermions plus a visible photon, i.e. $e^+e^- \to 4f+\gamma$, are a building block of the full $O(\alpha)$ electroweak corrections to $4f$ processes, providing the hard bremsstrahlung contribution. Furthermore, radiative $4f$ processes are also an interesting physics subject by themselves, since the luminosity achieved at LEP makes them directly accessible to the experimental investigation, as recently discussed in [3–5], where first results on the measurement of the $W^+W^-\gamma$ cross section have been reported.

A very peculiar feature of the processes under consideration is that they give the opportunity of directly testing the non-abelian structure of the gauge boson self-interactions. Actually, as other processes studied at LEP, such as $e^+e^- \to W^+W^- \to 4f$, $e^+e^- \to We\nu_e$ (single-W production) and $e^+e^- \to \nu\bar{\nu}\gamma$, $e^+e^- \to 4f+\gamma$ reactions are sensitive to trilinear gauge couplings (TGC). More importantly, they can be used to test quartic gauge couplings (QGC), since they are, together with $\nu\bar{\nu}\gamma\gamma$ final states, the only accessible LEP2 processes that contain quartic gauge boson vertices with at least one photon at tree level [5]. Quartic vertices involving only massive gauge bosons give rise to six-fermion final states and are outside the sensitivity of LEP, being accessible only at the energies of a future e^+e^- linear collider (LC). Both charged current (CC) radiative $4f$ processes, mediated by two W bosons, and neutral current (NC) ones, mediated by two Z bosons, are in principle suitable to examine the effect of possibly anomalous gauge couplings (AGC). In this work particular attention is paid to CC processes, because of the larger cross section of $WW\gamma$ events with respect to $ZZ\gamma$ final states.

The first tree-level calculations of $e^+e^- \to 4f+\gamma$ processes were performed in [6,7]. In these papers all electroweak contributions as well as fermion mass effects were accounted for by exploiting different approaches to the automatic calculation of the exact tree-level matrix element [8,9]. Since then, some event generators for the simulation of $4f+\gamma$ events in e^+e^- collisions have been developed: RacoonWW [10], a generator based on the calculation of all $4f+\gamma$ final states in the massless approximation [11]; CompHEP [12] and grc4f [13], which are general-purpose packages relying upon the automatic calculation of tree-level amplitudes (including fermion masses) and phase space; Helac/Phegas [14], a program implementing a recursive algorithm for the calculation of the scattering amplitudes. The interested reader is referred to [2] for more details. In addition to the above computational tools, also a calculation of the massive matrix element of $e^+e^- \to 4f+\gamma$ processes has recently appeared in the literature [15], accompanied by a detailed phenomenological analysis of fermion mass effects in $4f$ and $4f+\gamma$ final states at LEP2 energies [16]. In all the theoretical studies devoted so far to $4f+\gamma$ production, the effects of quartic anomalous gauge couplings (QAGC), which are a win-

dow on the mechanism of spontaneous symmetry breaking [17] and which are presently of special experimental interest, have not been taken into account. Actually, recent phenomenological studies on the subject of QAGC at high-energy e^+e^- colliders have been performed by considering three-vector boson $WW\gamma, ZZ\gamma, Z\gamma\gamma$ production and treating W, Z particles in the on-shell approximation [18,19]. Anomalous quartic couplings in $\nu\bar{\nu}\gamma\gamma$ production via WW fusion have been analyzed in [20]. Experimental searches for QAGC at LEP rely upon the theoretical results of [18–22] and make use of the computational tools of [18,20].

In the light of the present situation and in view of future measurements at LC, a full calculation of $e^+e^- \to 4f+\gamma$ processes, including the effects of AGC and of the most important radiative corrections, is desirable. This task is accomplished in the present paper, by presenting the new event generator WRAP (W Radiative process with ALPHA [9] and Pavia) for the simulation of $4f+\gamma$ processes at e^+e^- colliders. This program is based on the calculation of exact matrix elements, including the effect of fermion masses, both for CC and NC processes. Charged trilinear anomalous gauge couplings (TAGC) and the genuinely QAGC, i.e. those giving no contributions to trilinear vertices, are included in the calculation, as well as the large effect of initial state radiation (ISR). A tuned comparison between the predictions of a preliminary version of WRAP and of the other two event generators RacoonWW and Helac/Phegas can be found in [2].

This paper is organized as follows. In Sect. 2 the main features of the calculation are described. After the description of the treatment of the multi-particle phase space, the theoretical details concerning the calculation of the exact matrix elements, the implementation of anomalous gauge couplings and ISR are given. A sample of numerical results as obtained by means of the Monte Carlo WRAP is presented in Sect. 3, paying particular attention to the contribution of fermion masses, to the impact of ISR and to the effects of AGC at LEP2 and LC energies. Conclusions are drawn and possible perspectives are sketched in Sect. 4.

2 Features of the calculation

2.1 Phase space integration

The kinematics of the $2 \to 5$ particles processes has been treated generating the 5-body phase space recursively, since the process can be seen as production and subsequent decay of a pair of massive gauge bosons.

Concerning CC-like processes, the configurations of interest are related to a photon emitted from the initial state (see Fig. 1), from an intermediate W boson (see Fig. 2) and from the final state charged fermions (see Fig. 3). As far as emission from the initial state is concerned, the adopted phase space decomposition reads as follows:

$$\begin{aligned} \mathrm{d}\Phi_5 = {} & (2\pi)^6 \mathrm{d}\Phi_3(P; p_5, Q_{V_1}, Q_{V_2}) \mathrm{d}\Phi_2(Q_{V_1}; p_1, p_2) \\ & \times \mathrm{d}\Phi_2(Q_{V_2}; p_3, p_4) \mathrm{d}Q^2_{V_1} \mathrm{d}Q^2_{V_2}, \end{aligned} \tag{1}$$

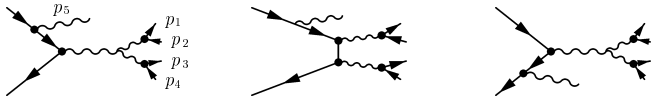

Fig. 1. Example of Feynman diagrams for photon radiation from the initial state

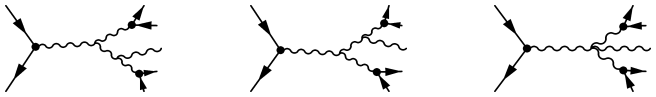

Fig. 2. Example of Feynman diagrams for photon radiation from W bosons

Fig. 3. Example of Feynman diagrams for photon radiation from final state fermions

where V_1 and V_2 indicate the W gauge bosons, the momenta p_i with $i = 1, \ldots, 4$ stand for the momenta of the final state fermions and p_5 is the photon momentum. The eleven independent variables have been chosen to be

(1) photon variables E_γ, θ_γ and ϕ_γ in the c.m. frame;
(2) invariant mass squared $Q^2_{V_1}$ and $Q^2_{V_2}$;
(3) three θ and ϕ angle pairs in the rest frame of each decaying "particle", namely in the frames given by the conditions $\boldsymbol{P} - \boldsymbol{p}_5 = \boldsymbol{0}$, $\boldsymbol{Q}_{V_1} = \boldsymbol{0}$ and $\boldsymbol{Q}_{V_2} = \boldsymbol{0}$.

When the photon is emitted from the final state, which means for a CC process from a virtual W or from a virtual charged fermion, the following decomposition can be considered for convenience:

$$\begin{aligned} \mathrm{d}\Phi_5 = {} & (2\pi)^6 \mathrm{d}\Phi_2(P; Q_{V_1}, Q_{V_2}) \mathrm{d}\Phi_3(Q_{V_1}; p_5, p_1, p_2) \\ & \times \mathrm{d}\Phi_2(Q_{V_2}; p_3, p_4) \mathrm{d}Q^2_{V_1} \mathrm{d}Q^2_{V_2}. \end{aligned} \tag{2}$$

In the case of the photon emitted from an internal gauge boson the independent variables can be chosen as follows:

(1) photon variables E_γ, θ_γ and ϕ_γ in the c.m. frame;
(2) invariant mass squared $Q^2_{V_1}$ and $Q^2_{V_2}$;
(3) one θ and ϕ W-angle pair in the c.m. frame;
(4) two θ and ϕ angle pairs for $\boldsymbol{p}_1$ and $\boldsymbol{p}_3$ in the rest frame of the bosons V_1 and V_2, respectively.

In the case of photon emission from a final state fermion the following independent variables can be adopted:

(1) invariant mass squared $Q^2_{V_1}$ and $Q^2_{V_2}$;
(2) one θ and ϕ W-angle pair in the c.m. frame;
(3) one θ and ϕ angle pair for $\boldsymbol{p}_3$ in the rest frame of the boson V_2;
(4) energies of p_1 and p_5 momenta in the c.m. frame;
(5) azimuthal angle ϕ of p_1 in the rest frame of V_1;
(6) ϕ_γ in the rest frame of the radiating fermion;
(7) $\cos\theta_{\gamma\text{-}f}$ in the c.m. frame,

where $\theta_{\gamma\text{-}f}$ is the relative angle between the radiating fermion and the photon.

An analogous phase space parameterization has been implemented in WRAP for the case of NC processes, neglecting of course the channels related to the photonic emission from internal lines. The above phase-pace decompositions, iterated for each possible radiation pattern, give rise to several channels, depending on the final state considered.

In the previous formulas $\mathrm{d}\Phi_n$ represents the element of n-body phase space given by

$$\mathrm{d}\Phi_n(P;p_1,\ldots,p_n) = (2\pi)^4\delta^4\left(P-\sum_{i=1}^{n}p_i\right)\prod_{i=1}^{n}\frac{\mathrm{d}^3p_i}{(2\pi)^3 2E_i}. \quad (3)$$

The code works taking into account all the configurations discussed above according to a standard multichannel Monte Carlo approach [23].

In order to perform an efficient event generation, the peaking behavior of the matrix element has been treated in the following way:

(1) the squared invariant masses of the massive gauge bosons V are sampled according to a Breit–Wigner distribution centered around M_V^2, while the photon propagator is sampled according to the $1/Q^2$ distribution;
(2) the infrared divergence is sampled according to a $1/E_\gamma$ distribution;
(3) the collinear peak arising from the photon emission due to an external charged fermion is brought under control by sampling it with a distribution proportional to $1/(1-\beta\cos\theta)$, where θ is the separation angle between the radiating fermion and the photon, and $\beta=(1-m^2/E^2)^{1/2}$, m and E being the mass and the energy of the fermion respectively.

For a realistic account of gauge boson properties, and to avoid integration singularities, it is mandatory to include the gauge boson width in the propagators. The so-called fixed-width scheme [10,24] is adopted in WRAP. Actually, as shown in [10], the fixed-width scheme, even if it violates $SU(2)$ gauge invariance, is a reliable $U(1)$ gauge-restoring method and is able to guarantee predictions for $e^+e^-\to 4f+\gamma$ processes in good numerical agreement with a scheme preserving all the relevant Ward identities, such as the complex-mass scheme [10].

2.2 Tree-level matrix element

As already mentioned, the present work is based on the calculation of the *fully massive* Born matrix element of $e^+e^-\to 4f+\gamma$ processes. The exact matrix elements for CC and NC $e^+e^-\to 4f+\gamma$ processes are available in WRAP. The calculation is performed by using ALPHA [9], an iterative algorithm for the automatic evaluation of tree-level scattering amplitudes without using Feynman graphs (see [25] for a review of the method and of recent phenomenological applications). For the processes under consideration, a completely numerical approach turns out to be particularly convenient not only for the very large amount of contributing Feynman diagrams, but also because the calculation can be performed in the presence of fermion masses without any additional complication. This is of special importance for $4f+\gamma$ final states involving muons, where the separation angle between muon and photon can be realistically set to zero, and a calculation taking into account the finite muon mass is mandatory, to avoid collinear singularities.

2.3 Anomalous gauge couplings

Information about the structure of TGC and QGC can be obtained by the analysis of $4f+\gamma$ production processes. In particular, CC radiative $4f$ processes, although characterized by a lower statistics, are potentially a complementary channel to the $4f$ final states in order to test the effect of TGC, because of the larger amount of diagrams involving trilinear gauge interactions. More importantly, $4f+\gamma$ processes are interesting in order to put bounds on deviations from standard quartic gauge couplings. In the following, the theoretical details of the parameterization adopted in order to keep under control this important phenomenological issue are described.

2.3.1 Trilinear anomalous gauge couplings

It is possible to take into account the effect of charged TGC (anomalous and not anomalous) by means of the following lagrangian [26,27]:

$$\begin{aligned}\mathrm{i}L_{\mathrm{TGC}} &= g_{WWV}\,[\,g_1^V V^\mu\left(W^-_{\mu\nu}W^{+\nu}-W^+_{\mu\nu}W^{-\nu}\right)\\ &\quad+\kappa_V W^+_\mu W^-_\nu V^{\mu\nu}+\frac{\lambda_V}{m_W^2}V^{\mu\nu}W^{+\rho}_\mu W^-_{\rho\nu}\\ &\quad+\mathrm{i}g_5^V\varepsilon_{\mu\nu\rho\sigma}\left(\left(\partial^\rho W^{-\mu}\right)W^{+\nu}-W^{-\mu}\left(\partial^\rho W^{+\nu}\right)\right)V^\sigma\,],\\ &\quad V=\gamma,Z, \end{aligned} \quad (4)$$

which represents the most general lagrangian describing trilinear WWV gauge interactions, with the exception of the operators violating C, P and CP symmetries. L_{TGC} has been implemented in ALPHA, and the presence of anomalous couplings can be studied, as done at LEP [28], by using the relations [27,29]

$$\Delta\kappa_\gamma=-\frac{c_W^2}{s_W^2}(\Delta\kappa_Z-\Delta g_1^Z),\quad \lambda_Z=\lambda_\gamma\equiv\lambda, \quad (5)$$

where $\Delta\kappa_V=\kappa_V-1$ and $\Delta g_1^Z=g_1^Z-1$. The standard model (SM) Lagrangian is recovered for $g_1^V=k_V=1$, $\lambda=0$, $g_5^V=0$. Triple anomalous neutral gauge couplings, considered in [30] and looked for at LEP in $e^+e^-\to Z\gamma, ZZ$ processes [31], are not presently taken into account.

2.3.2 Quartic anomalous gauge couplings

Quartic gauge couplings involving at least one photon are analyzed at LEP [5]. In particular, $W^+W^-\gamma\gamma$ and

$W^+W^-Z\gamma$ vertices are probed in $WW\gamma \to 4f+\gamma$ and $\nu\bar{\nu}\gamma\gamma$ final states [3,4], while $e^+e^- \to Z\gamma\gamma$ processes [32] are investigated to put bounds on the $ZZ\gamma\gamma$ vertex, which is a gauge interaction not predicted by SM at tree level. In the present work the operators considered in [19] for genuine anomalous quartic couplings containing at least one photon, namely $W^+W^-Z\gamma$, $W^+W^-\gamma\gamma$ and $ZZ\gamma\gamma$ vertices, have been implemented in ALPHA, upgrading the version used in [33] for the analysis of QAGC in six-fermion final states at the energies of future linear colliders. The implemented lagrangian includes all the relevant six-dimensional operators and reads as follows:

$$L_{\mathrm{QGC}} = W_1 + W_2 + Z_1 + Z_2 + W_0^Z + W_c^Z + W_1^Z + W_2^Z + W_3^Z. \quad (6)$$

In the above equation the Lorentz structure of the operators is given by

$$\begin{aligned} W_1 &= a_{w1} F_{\mu\nu} F^{\mu\nu} W_\rho^+ W^{-\rho}, \\ W_2 &= a_{w2} F_{\mu\nu} F^{\mu\rho} W^{+\nu} W_\rho^- + \mathrm{h.c.}, \\ Z_1 &= a_{z1} F_{\mu\nu} F^{\mu\nu} Z_\rho Z^\rho, \\ Z_2 &= a_{z2} F_{\mu\nu} F^{\mu\rho} Z^\nu Z_\rho, \\ W_0^Z &= a_{wz0} F_{\mu\nu} Z^{\mu\nu} W_\rho^+ W^{-\rho}, \\ W_c^Z &= a_{wzc} F_{\mu\nu} Z^{\mu\rho} W^{+\nu} W_\rho^- + \mathrm{h.c.}, \\ W_1^Z &= a_{wz1} F_{\mu\nu} W^{+\mu\nu} Z^\rho W_\rho^- + \mathrm{h.c.}, \\ W_2^Z &= a_{wz2} F_{\mu\nu} W^{+\mu\rho} Z^\nu W_\rho^- + \mathrm{h.c.}, \\ W_3^Z &= a_{wz3} F_{\mu\nu} W^{+\mu\rho} Z_\rho W^{-\nu} + \mathrm{h.c.}, \end{aligned} \quad (7)$$

where the a_i are coefficients of dimension M^{-2}. It is worth noticing that, by imposing appropriate relations between the a_i's, symmetry properties, such as for instance $SU(2)_{\mathrm{c}}$ custodial symmetry or $SU(2)\times U(1)$ gauge invariance, can be guaranteed, as shown in [19]. In the parameterization adopted in [19] the a_i are real coefficients whose explicit expression can be directly read off from the corresponding operator structure of [19] itself. In particular, the coefficients a_0 and a_c, originally introduced in [21] and related to the $WW\gamma\gamma$ and $ZZ\gamma\gamma$ structure, can be obtained from the above a_i coefficients by means of the following relations:

$$\begin{aligned} a_{w1} &= -\frac{e^2}{8\Lambda^2} a_0, \\ a_{z1} &= -\frac{e^2}{16\cos^2\theta_{\mathrm{w}}\Lambda^2} a_0, \\ a_{w2} &= -\frac{e^2}{16\Lambda^2} a_c, \\ a_{z2} &= -\frac{e^2}{16\cos^2\theta_{\mathrm{w}}\Lambda^2} a_c, \end{aligned} \quad (8)$$

where Λ represents a scale of new physics. As far as the $WWZ\gamma$ vertex is concerned, an additional structure has been proposed in the literature [18,22], whose expression can be derived from the above a_i coefficients by means of the following relations:

$$\begin{aligned} a_{wzc} &= \mathrm{i}\frac{e^2}{16\cos\theta_{\mathrm{w}}\Lambda^2} a_n, \\ a_{wz2} &= \mathrm{i}\frac{e^2}{16\cos\theta_{\mathrm{w}}\Lambda^2} a_n, \\ a_{wz3} &= -\mathrm{i}\frac{e^2}{16\cos\theta_{\mathrm{w}}\Lambda^2} a_n. \end{aligned} \quad (9)$$

On the experimental side, bounds on a_0, a_c and a_n couplings are quoted by LEP collaborations via the analysis of $WW\gamma$ and $\nu\bar{\nu}\gamma\gamma$ final states [3–5]. It is worth noticing, in passing, that, thanks to the implementation of the lagrangian of (6) in the ALPHA code, an improved version of the Monte Carlo generator NUNUGPV [34,35] is also available for the study of QAGC in $\nu\bar{\nu}\gamma\gamma$ events.

The result of the implementation in ALPHA has been carefully cross-checked by an independent analytical calculation of all $V_1V_2 \to V_3V_4$ amplitudes, with $V_i = \gamma, W, Z$. The check has been performed for all the processes obtained from $W^+W^- \to Z\gamma$ scattering, by permutating particles.

2.4 Initial-state radiation

In order to match the precision of LEP measurements, the most important radiative corrections have to be considered. Among them, it is well known that undetected initial state radiation (ISR) plays a major rôle. It can be taken into account in the leading log approximation by using the QED structure function (SF) approach, in terms of collinear [36] or $p_\perp$-dependent SF [34,35]. Following recent work done in [35], both prescriptions are available in WRAP, for the reason explained below. When ISR is included via collinear SF, the QED corrected cross section can be written as

$$\sigma_{\mathrm{QED}}^{4f+1\gamma}(s) = \int \mathrm{d}x_1 \mathrm{d}x_2 D(x_1,s) D(x_2,s) \mathrm{d}\sigma_0^{4f+1\gamma}(x_1x_2s), \quad (10)$$

by convoluting the tree-level cross section with electron SF. However, due to the presence of an observed photon in the hard-scattering matrix element, the inclusion of ISR needs some care. Actually, since the collinear SF can be viewed as the result of an integration over the angular variables of the photon radiation, an overlapping between the detected kernel photon and pre-emission photons at large angle may occur[1]. The consequence is that a double counting takes place if higher-order QED corrections are naively included by using collinear SF [35].

On the other hand, it is expected that the bulk of the correction is well estimated by collinear SF, since the emission of a photon from an on-shell initial state fermion is almost collinear. However, in order to provide a more appropriate treatment of photon corrections and give an estimate of the double-counting effect, the SF method can be improved by means of the use of $p_\perp$-dependent SF,

[1] The same problem is discussed in detail in [35] for the process $e^+e^- \to \nu\bar{\nu} + n\gamma$. We refer the reader to [35] for more details on the strategy here adopted

Table 1. Comparison between WRAP and RacoonWW predictions for the massless Born cross section of NC processes at $s^{1/2} = 190\,\mathrm{GeV}$. Input parameters and cuts as in [10]

Cross section (fb)	WRAP	RacoonWW
$\mu^+\mu^-\tau^+\tau^-\gamma$	6.76 ± 0.03	6.78 ± 0.03
$\mu^+\mu^-\nu_\tau\bar{\nu}_\tau\gamma$	4.248 ± 0.009	4.259 ± 0.009
$\mu^+\mu^-u\bar{u}\gamma$	12.65 ± 0.03	12.70 ± 0.04

i.e. by generating angular variables for the ISR photons according to $1/(p \cdot k)$, which is the leading behavior for radiation of momentum k emitted by an on-shell fermion of momentum p. In such a scheme, the QED corrected cross section can be calculated as

$$\sigma_{\mathrm{QED}}^{4f+1\gamma} = \int \mathrm{d}x_1\mathrm{d}x_2 \int_{\Omega_c} \mathrm{d}c_\gamma^{(1)}\mathrm{d}c_\gamma^{(2)} \times \tilde{D}(x_1, c_\gamma^{(1)}; s)\tilde{D}(x_2, c_\gamma^{(2)}; s)\mathrm{d}\sigma^{4f+1\gamma}, \quad (11)$$

where $D(x, c_\gamma; s)$ is the $p_\perp$-dependent SF [34]. According to (11), an "equivalent " photon is generated and accepted as an ISR contribution only if it satisfies a rejection algorithm based on the following requirements:

(1) the energy of the "equivalent" photon is below the energy threshold for the observed photon, for arbitrary angles; or
(2) the "equivalent" photon is collinear to a charged particle (i.e. under the minimum separation angle required in order to be detected), for arbitrary energies.

Within the angular acceptance of the observed photon, the cross section is computed by means of the exact matrix element for the considered $4f + \gamma$ final state. Therefore, (11) applies to the signature of four fermions plus an isolated hard photon, corrected by the effect of undetected soft and/or collinear radiation. Aiming to obtain a correct evaluation of the size of the double-counting effects, a limit of the present treatment of undetected radiation is that only ISR is actually considered. This issue could be addressed in a more complete way by using, for example, a QED parton shower approach as developed in [37], in order to describe the radiation from all external charged legs, thus including the contribution of undetected final state radiation.

3 Numerical results

The aim of the present section is to give some details on the technical precision of WRAP and discuss the impact of the effects due to fermion masses, ISR and AGC on observables of experimental interest.

In order to test the reliability and the theoretical accuracy of the event generators, a detailed tuned comparison between the predictions of WRAP and other available programs have been carried out in the context of the four-fermion working group of the LEP2 Monte Carlo workshop at CERN [2]. The comparisons, referred to integrated cross sections and differential distributions of several CC processes, showed perfect technical agreement. The comparison is here extended to NC processes, as shown in Table 1, between the predictions of WRAP and RacoonWW with input parameters and cuts as in [10]. As can be seen, also for NC final states the agreement is excellent. A further comparison between the predictions of WRAP and those of [16] is reported in Table 2, for several cross sections of CC and NC processes, in the presence of finite fermion masses and in terms of the same input parameters and cuts as adopted in [16]. Perfect agreement is registered for all the considered $4f + \gamma$ final states.

Table 2. Comparison between WRAP and the predictions of [16] for the massive Born cross section of CC and NC processes at $s^{1/2} = 190\,\mathrm{GeV}$. Input parameters and cuts as in [16]

Cross section (fb)	WRAP	[16]
$u\bar{d}e^-\bar{\nu}_e\gamma$	220.1 ± 0.5	220.3 ± 0.7
$c\bar{s}e^-\bar{\nu}_e\gamma$	217.5 ± 0.4	218.2 ± 0.7
$\mu^+\bar{\nu}_\mu e^-\bar{\nu}_e\gamma$	78.6 ± 0.1	79.0 ± 0.3
$\tau^+\bar{\nu}_\tau e^-\bar{\nu}_e\gamma$	77.6 ± 0.2	77.5 ± 0.2
$u\bar{d}\mu^-\bar{\nu}_\mu\gamma$	213.0 ± 0.1	213.8 ± 0.3
$u\bar{d}\tau^-\bar{\nu}_\tau\gamma$	208.7 ± 0.4	209.3 ± 0.5
$\tau^+\bar{\nu}_\tau\mu^-\bar{\nu}_\mu\gamma$	75.2 ± 0.1	75.1 ± 0.2
$u\bar{d}s\bar{c}\gamma$	590.0 ± 0.6	593 ± 2
$\mu^+\mu^-\nu_\tau\bar{\nu}_\tau\gamma$	5.32 ± 0.02	5.32 ± 0.03
$\tau^+\tau^-\mu^+\mu^-\gamma$	4.15 ± 0.02	4.18 ± 0.02
$\tau^+\tau^-\nu_\mu\bar{\nu}_\mu\gamma$	3.175 ± 0.006	3.167 ± 0.007

The phenomenological analysis makes use of the following input parameters:

$$\begin{aligned} &G_{\mathrm{F}} = 1.16637 \cdot 10^{-5}\,\mathrm{GeV}^{-2}, && M_Z = 91.1867\,\mathrm{GeV}, \\ &M_W = 80.35\,\mathrm{GeV}, && \sin^2\theta_{\mathrm{w}} = 1 - M_W^2/M_Z^2, \\ &\Gamma_Z = 2.49471\,\mathrm{GeV}, && \Gamma_W = 2.04277\,\mathrm{GeV}, \\ &m_\mu = 0.10565839\,\mathrm{GeV}, && m_s = 0.15\,\mathrm{GeV}, \\ &m_c = 1.55\,\mathrm{GeV}. \end{aligned} \quad (12)$$

The form used for the propagator of the massive gauge bosons is, according to the fixed-width scheme, $\sim 1/(p^2 - M^2 + \mathrm{i}\Gamma M)$. The processes considered are the radiative semi-leptonic final states of the kind $e^+e^- \to l^+\nu_l q\bar{q}'\gamma$. The cuts adopted are

$$\begin{aligned} &|\cos\theta_\gamma| \le 0.985, && E_\gamma \ge 1\,\mathrm{GeV}, \\ &|\cos\theta_l| \le 0.985, && E_l \ge 5\,\mathrm{GeV}, \\ &\theta_{\gamma\text{-}f} \ge 5^\circ, \\ &M_{q\bar{q}'} \ge 10\,\mathrm{GeV}, \end{aligned} \quad (13)$$

where $\theta_{\gamma(l)}$ is the photon (lepton) scattering angle, $E_{\gamma(l)}$ is the photon (lepton) energy, $\theta_{\gamma\text{-}f}$ is the angular separation between photon and final charged fermions, and $M_{q\bar{q}'}$ is the $q\bar{q}'$ invariant mass.

Table 3 shows the effect of fermion masses on integrated cross sections at $s^{1/2} = 200\,\mathrm{GeV}$ for two different photon–fermion separation angles. In the first row, the angular separation $\theta_{\gamma-f}$ between photon and all charged

Table 3. Comparison between massive and massless Born cross section for the final state $\mu^+\nu_\mu\bar{c}s+\gamma$ at $s^{1/2}=200\,\mathrm{GeV}$. $\theta_{\gamma-f}$ is the minimum separation angle between the photon and final state charged fermions; other cuts as in (13). The first line refers to the massive case, the second one to the massless approximation

$\theta_{\gamma-f}$ (deg)	Cross section (fb)
5°	74.294 ± 0.029
	75.732 ± 0.022
1°	93.764 ± 0.037
	100.446 ± 0.037

Table 4. Comparison between massive and massless Born cross sections for the final state $\mu^+\nu_\mu\bar{c}s+\gamma$ at $s^{1/2}=200\,\mathrm{GeV}$. $\theta_{\gamma-f}$, with $f=q,\mu$, is the minimum separation angle between the photon and final state charged fermions; other cuts as in (13). In the third column, the first result refers to the massive case, and the second one to the massless case. The relative difference is shown in the last column. See also [2]

$\vartheta_{\gamma-q}$ (deg)	$\vartheta_{\gamma\text{-}\mu}$ (deg)	Cross section (fb)	δ (%)
5°	1.0°	90.157 ± 0.036	1.92 ± 0.08
		91.903 ± 0.035	
5°	0.1°	104.777 ± 0.046	9.31 ± 0.09
		115.004 ± 0.044	
5°	0.0°	105.438 ± 0.045	

final state fermions is fixed at 5°, while in the second row $\theta_{\gamma-f}=1°$. As expected, the relative difference between the massless and massive cross section increases, going from 2% of the first row to the 7% of the second row, because of the importance of fermion mass contributions when the photon approaches the collinear region around an on-shell charged particle. In the case of a final state containing a muon, the separation angle $\vartheta_{\gamma-f}$ can be realistically set to zero, because of different behavior of photons and muons in the experimental apparatus. Table 4 shows the difference between massive and massless cross section, with the minimal separation between quarks and photon fixed at 5° and progressively relaxing the separation cut between muon and photon. It can be seen that the massless calculation is still reliable for 1° of minimum separation, the relative difference being around 2%, but it becomes inadequate when the separation falls at some fraction of degree, the relative difference being of the order of 10%. Therefore, in particularly stringent experimental conditions, only a massive $4f+\gamma$ calculation can provide reliable predictions in the presence of muons in the final state.

Figure 4 shows the line shape of the cross sections of the radiative semi-leptonic processes $\mu^+\nu_\mu\bar{u}d+\gamma$ and $e^+\nu_e\bar{u}d+\gamma$, as a function of the c.m. energy in the LEP2 range. The QED corrected cross section via collinear SF for the $\mu^+\nu_\mu\bar{u}d+\gamma$ final state is also plotted. The comparison shows that the contribution due to the additional

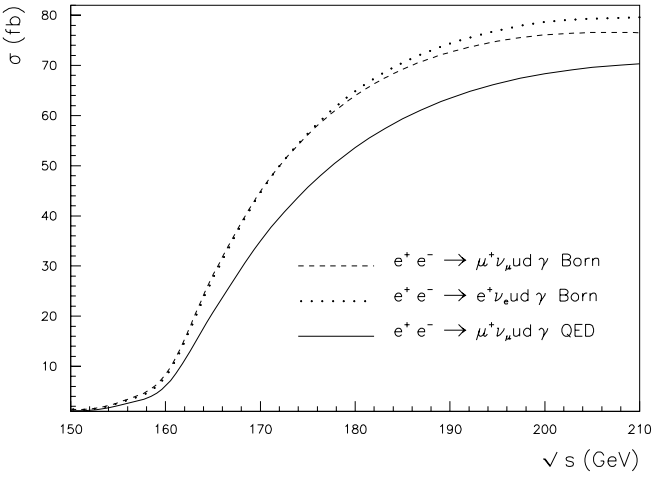

Fig. 4. Cross section for the semi-leptonic processes $e^+e^-\to l^+\nu_l\bar{u}d\gamma$ with $l^+=\mu^+$ (dashed line) and $l^+=e^+$ (dotted line). The solid line shows the QED corrected cross section via collinear SF for the $\mu^+\nu_\mu\bar{u}d\gamma$ final state. See also [2]

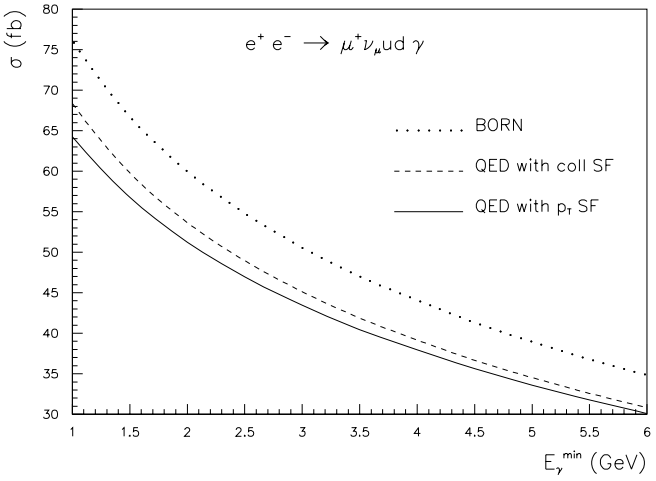

Fig. 5. Comparison between collinear (dashed line) and $p_\perp$-dependent (solid line) SF on the cross section of the process $e^+e^-\to\mu^+\nu_\mu\bar{u}d\gamma$, as a function of the energy threshold of the visible photon $E_\gamma^{\min}$. The dotted line is the Born prediction. See also [2]

t-channel diagrams present in the $e^+\nu_e\bar{u}d+\gamma$ final state is not particularly relevant for the adopted selection criteria, the differences between the cross sections of the two processes being small. Concerning ISR in the strictly collinear approximation, its impact on the cross section is at the level of 10–15%, which is a phenomenologically relevant effect in the light of the LEP experimental accuracy. It is worth noticing that this result, obtained by means of a standard treatment of ISR as typically adopted in the experimental analysis of QAGC in radiative events at LEP [3,4], just provides the bulk of the effect due to ISR but it is affected, as previously discussed and quantified below, by a double counting because of the presence of a radiative process as hard-scattering reaction.

The contribution of initial state photon radiation is also shown in Figs. 5, as a function of the threshold en-

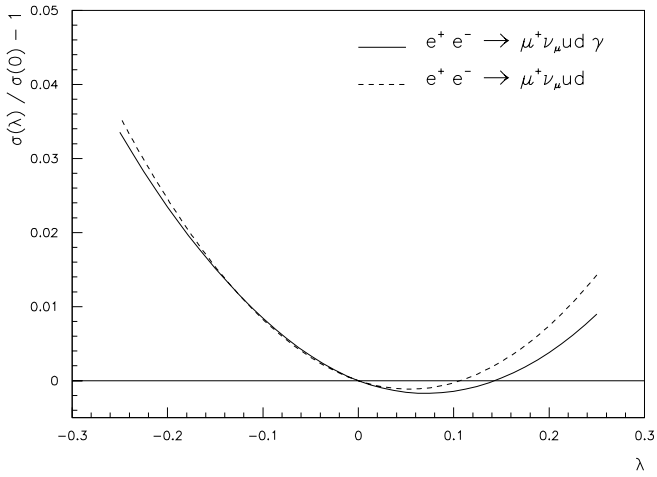

Fig. 6. The relative effect of TAGC λ on the cross section of the radiative process $e^+e^- \to \mu^+\nu_\mu\bar{u}d\gamma$ (solid line) and the corresponding $4f$ final state (dashed line)

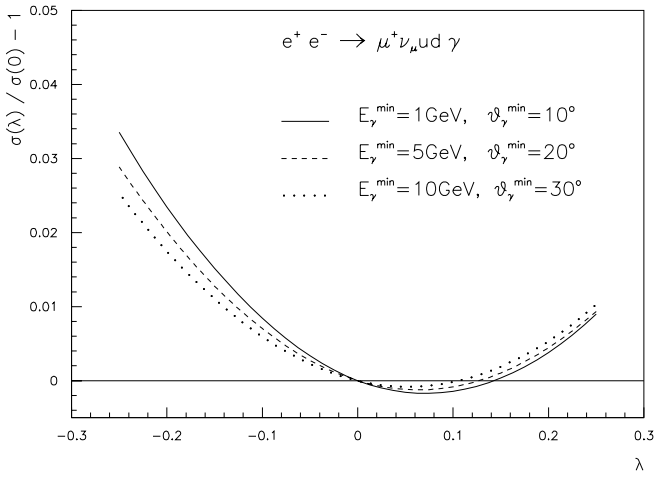

Fig. 7. The relative effect of TAGC λ on the cross section of the radiative process $e^+e^- \to \mu^+\nu_\mu\bar{u}d\gamma$ for different photon selection criteria

ergy $E_\gamma^{\min}$ of the observed photon. It can be noticed that the reduction factor due to collinear ISR is around 12–13%, almost independent of the photon detection threshold. However, as previously discussed, ISR in the collinear SF scheme introduces a double-counting effect when the pre-emission "equivalent" photon enters the phase space region of the kernel photon. In order to get an estimate of this overlapping contribution, the comparison of the corrections due to the collinear SF and $p_\perp$-dependent SF is shown. It is observed that the two prescriptions can differ at the 5% level for $E_\gamma^{\min}$ close to 1–2 GeV, while the difference becomes smaller and smaller as $E_\gamma^{\min}$ increases. Numerical investigation points out that, as expected, the discrepancy between collinear and $p_\perp$-dependent SF is larger near the soft and collinear region and at the level of some percent, thus yielding an estimate of the size of the double-counting effect at the level of ISR. Therefore, in the presence of particularly stringent experimental constraints sensitive to the soft and collinear emission, precise predictions demand a treatment of ISR that is able to keep under control the transverse degrees of freedom of photon radiation.

Let us proceed to the discussion of the effects due to (a sample of) AGC. Both integrated cross sections (Figs. 6–9) and differential distributions (Figs. 10–13) are considered. In Figs. 6–7 the (relative) effect of the TAGC λ on the $e^+e^- \to \mu^+\nu_\mu\bar{u}d\gamma$ cross section is examined, by plotting the relative difference between the cross section in the presence of a non-vanishing λ coupling and the SM cross section ($\lambda = 0$), as a function of the λ value at $s^{1/2} = 192$ GeV. Figure 6 shows a comparison of the effect of the λ coupling on the radiative $\mu^+\nu_\mu\bar{u}d+\gamma$ process and the corresponding $4f$ final state, which, as already remarked, differ as regards their content of trilinear gauge interactions. The numerical results for the $4f$ process have been obtained by means of the program WWGENPV [38]. For the considered λ values, the relative contribution is almost the same on the two processes (obviously the cross sections are quite different), giving a difference at 2–3% level only for extreme λ values. Therefore, in the presence of standard cuts on the observed photon, trilinear gauge interactions due to W radiation in radiative $4f$ processes do not enhance the sensitivity to TAGC with respect to a pure $4f$ final state. This conclusion is further corroborated by the results shown in Fig. 7, where the effect of the λ coupling is studied for different photon cuts, with the aim of suppressing the mostly collinear fermion radiation by imposing more and more severe cuts on the detected photon. By comparing the relative deviations shown in Figs. 6 and 7, one can conclude that in radiative $4f$ processes W radiation can be hardly disentangled from the radiation off fermions, the observed deviations being almost at the same level for all the set of cuts considered.

The effect of the QAGC k_0^W, as defined in [19], is shown in Figs. 8 and 9 for the process $\mu^+\nu_\mu\bar{u}d\gamma$, as a function of the parameter k_0^W at $s^{1/2} = 200$ GeV. For the scale of new physics Λ, the value $\Lambda = M_W$ is used, as conventionally done in the literature. Absolute and relative effects are shown in Figs. 8 and 9, respectively. In terms of the coefficients a_i of (7) the k_0^W coupling can be expressed as

$$a_{w1} = \frac{-e^2g^2}{2\Lambda^2}k_0^W\,,$$
$$a_{wz0} = \frac{-e^2g^2}{\Lambda^2}\frac{\cos\theta_{\rm w}}{\sin\theta_{\rm w}}k_0^W\,.$$

The solid line refers to the complete $4f+\gamma$ calculation of WRAP with input parameters and photon cuts as used in [19] and the additional cuts on fermions as given by (13). In order to compare with the results of [19], the dash-dotted line has been obtained by means of a calculation of the process $e^+e^- \to W^+W^-\gamma$ (performed independently and in agreement with the results of [19]), by taking into account the suitable branching ratios of the W bosons decaying into $\mu^+\nu_\mu$ and $\bar{u}d$ pairs. The dotted line is the prediction as obtained by WRAP, with additional cuts on the invariant masses of the two fermionic pairs con-

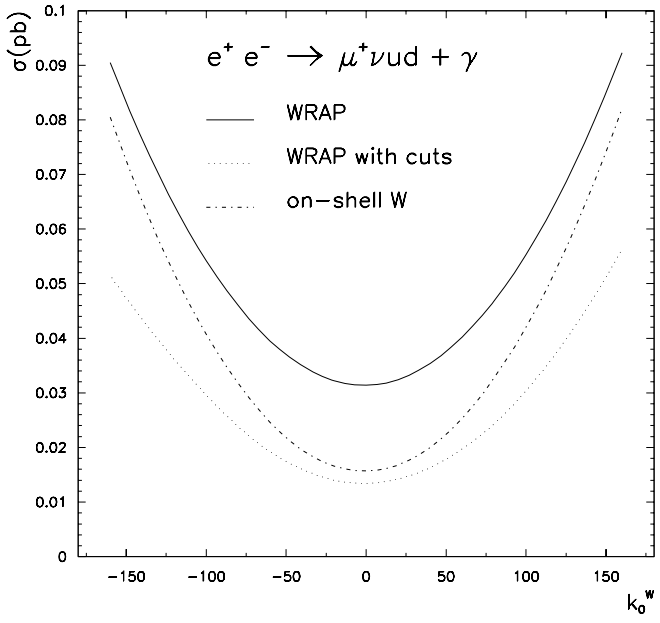

Fig. 8. The effect of the QAGC k_0^W at $s^{1/2} = 200\,\text{GeV}$ on the absolute cross section for the process $e^+e^- \to \mu^+\nu_\mu \bar{u}d + \gamma$, with $\Lambda = M_W$. The solid line is obtained by means of the full calculation of WRAP, the dash-dotted one with the real $WW\gamma$ approximation, and the dotted line refers to the calculation of WRAP with the additional cuts $75\,\text{GeV} \leq M(\mu^+\nu_\mu), M(\bar{u}d) \leq 85\,\text{GeV}$

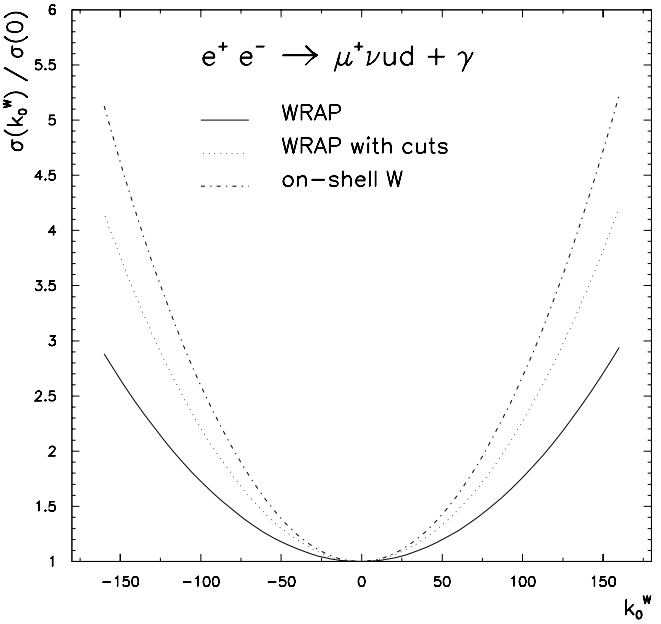

Fig. 9. The ratio between the cross section in the presence of a QAGC k_0^W and the SM cross section, as a function of k_0^W, for the three different cases as in Fig. 8

strained within 75 GeV and 85 GeV, in order to enhance, as much as possible, the contribution of diagrams with two resonant W bosons. It can be clearly noticed that, even in the presence of cuts on the invariant masses of the decay products, the complete $4f + \gamma$ calculation differ from the prediction of the $WW\gamma$ approximation, thus proving the importance of a full calculation for the extraction of meaningful limits on QAGC.

In Figs. 10–13 the most important photonic distributions are displayed using the code as event generator with the cuts of (13) at a typical LEP2 energy $s^{1/2} = 192\,\text{GeV}$. In each plot, the SM Born and the QED corrected predictions are compared with those obtained in the presence of AGC. The values used for the anomalous couplings are: $\lambda = -0.25$ and $k_0^W/\Lambda^2 = 0.01$. For the sake of comparison, all the data sample are normalized to the same luminosity. The $\cos\theta_\gamma$ distribution and the distribution of the cosine of the angle between the photon and the nearest charged particle are shown in Figs. 10 and 11, respectively. Typical peaking behavior in the close-to-collinear regions is clearly registered. In such regions, a particularly significant impact of the QACG k_0^W is also observed. Figures 12 and 13 refer to the E_γ and transverse photon momentum $p_\perp$ distribution, respectively, showing the characteristic infrared peak. As already noticed in [19], these observables turn out to be particularly sensitive to the presence of a QAGC in the region of high energy and $p_\perp$, the operator involved being of derivative type with respect to the photon field. In all the considered distributions, ISR introduce sizeable effects if compared with the deviations due to anomalous couplings.

Table 5. Effect of the QAGC $a_0/\Lambda^2, a_c/\Lambda^2, a_n/\Lambda^2$, with $\Lambda = M_W$, on the cross section of the process $e^+e^- \to u\bar{d}\mu^-\bar{\nu}_\mu\gamma$ at $s^{1/2} = 200\,\text{GeV}$

QAGC	Cross section (fb)
Standard model	76.0 ± 0.1
$a_0/\Lambda^2 = -0.01$	77.0 ± 0.1
$a_0/\Lambda^2 = +0.01$	77.2 ± 0.1
$a_c/\Lambda^2 = -0.01$	75.5 ± 0.1
$a_c/\Lambda^2 = +0.01$	76.9 ± 0.1
$a_n/\Lambda^2 = -0.01$	76.0 ± 0.1
$a_n/\Lambda^2 = +0.01$	76.0 ± 0.1

As far as the parameterization of QAGC in terms of a_0, a_c, a_n parameters is concerned, numerical results are shown in Tables 5 and 6, at $s^{1/2} = 200\,\text{GeV}$ and $s^{1/2} = 500\,\text{GeV}$, respectively. The cross sections in the presence of non-vanishing anomalous couplings are compared with the pure SM predictions. By looking at Tables 5 and 6, it can be noticed that the sensitivity of the $4f+\gamma$ processes to QAGC is much higher at the energies of a future LC than at LEP2, as a priori expected and already noticed in the literature for the $WW\gamma$ process [18,19].

4 Conclusions

The production of four fermions plus an additional detected photon in e^+e^- collisions is studied at LEP to test electroweak gauge boson couplings and in particular to derive bounds on QAGC. In order to provide predictions of

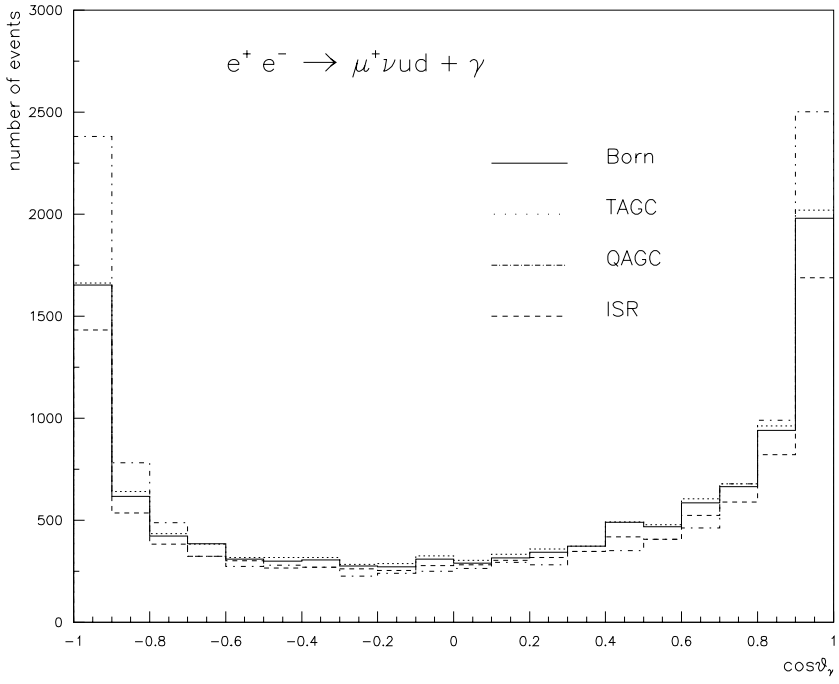

Fig. 10. The $\cos\theta_\gamma$ distribution for the process $e^+e^- \to \mu^+\nu_\mu\bar{u}d\gamma$ at $s^{1/2} = 192\,\mathrm{GeV}$. The Born approximation (solid line), the QED corrected calculation (dashed line), the predictions for $\lambda = -0.25$ (dotted line) and the ones for $k_0^W/\Lambda^2 = 0.01$ (dash–dotted line) are shown. Cuts as in (13)

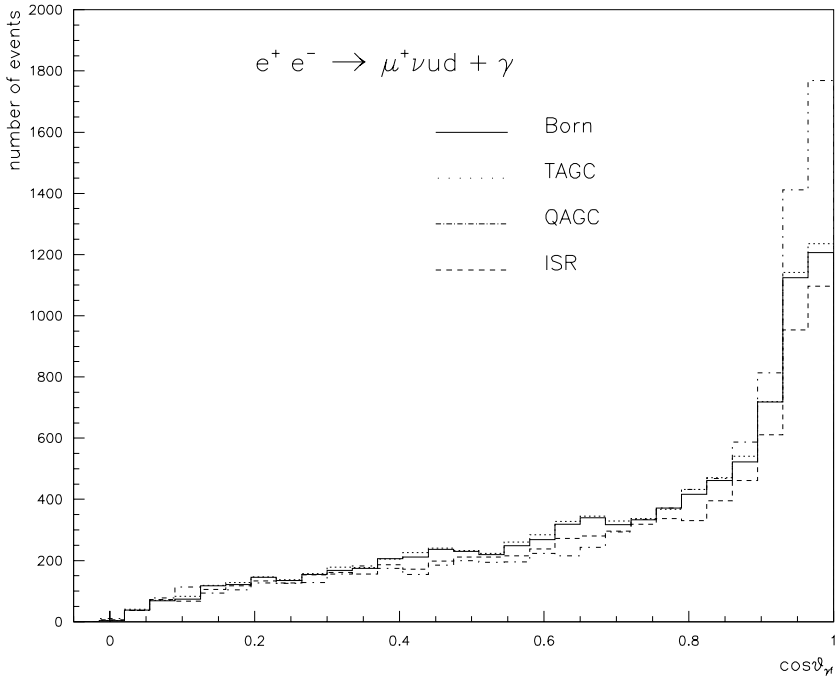

Fig. 11. The $\cos\theta_{\gamma f}$ distribution for the process $e^+e^- \to \mu^+\nu_\mu\bar{u}d\gamma$ at $s^{1/2} = 192\,\mathrm{GeV}$, where $\theta_{\gamma f}$ is the angle between the photon and the nearest charged particle. The samples are the same as in Fig. 10

Table 6. The same as in Table 5 at $s^{1/2} = 500\,\mathrm{GeV}$

QAGC	Cross section (fb)
Standard model	25.3 ± 0.1
$a_0/\Lambda^2 = -0.001$	83.8 ± 0.3
$a_0/\Lambda^2 = +0.001$	88.0 ± 0.2
$a_c/\Lambda^2 = -0.001$	41.3 ± 0.2
$a_c/\Lambda^2 = +0.001$	45.4 ± 0.2
$a_n/\Lambda^2 = -0.001$	26.4 ± 0.1
$a_n/\Lambda^2 = +0.001$	26.4 ± 0.1

phenomenological interest, an exact calculation of $4f + \gamma$ processes, including the effect of fermion masses, AGC and ISR has been performed. On the basis of the experimental accuracy, the contribution of fermion masses and ISR has been analyzed in comparison with typical deviations introduced by AGC. A new Monte Carlo event generator (WRAP) has been developed and is available for the simulation of radiative $4f$ events.

The main conclusions of the present study can be summarized as follows. The effect of finite fermion masses, as analyzed in the $\mu^+\nu_\mu\bar{c}s\gamma$ final state, turn out to be very

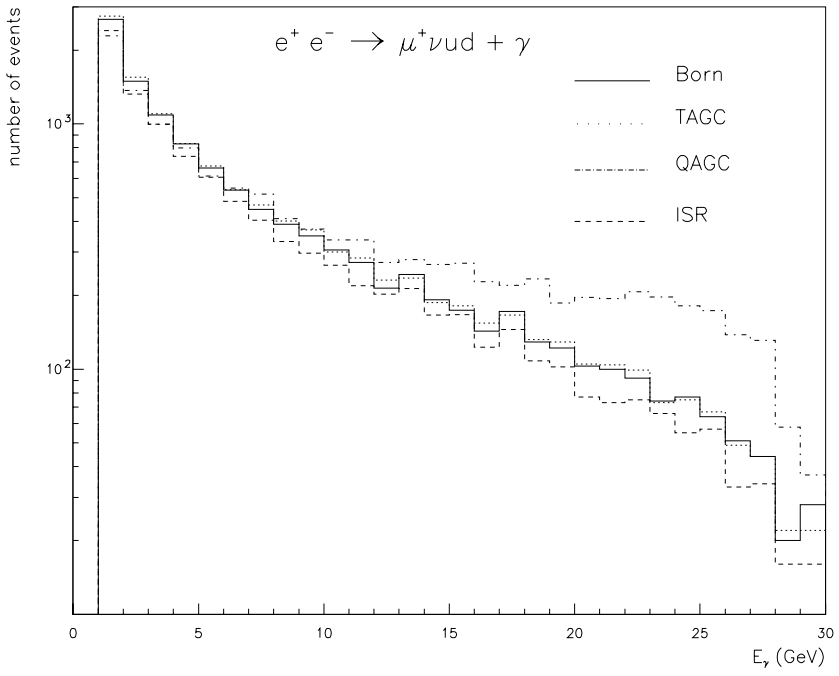

Fig. 12. The E_γ distribution for the process $e^+e^- \to \mu^+\nu_\mu\bar{u}d\gamma$ at $s^{1/2} = 192\,\mathrm{GeV}$ for the same sample of events as in Fig. 10

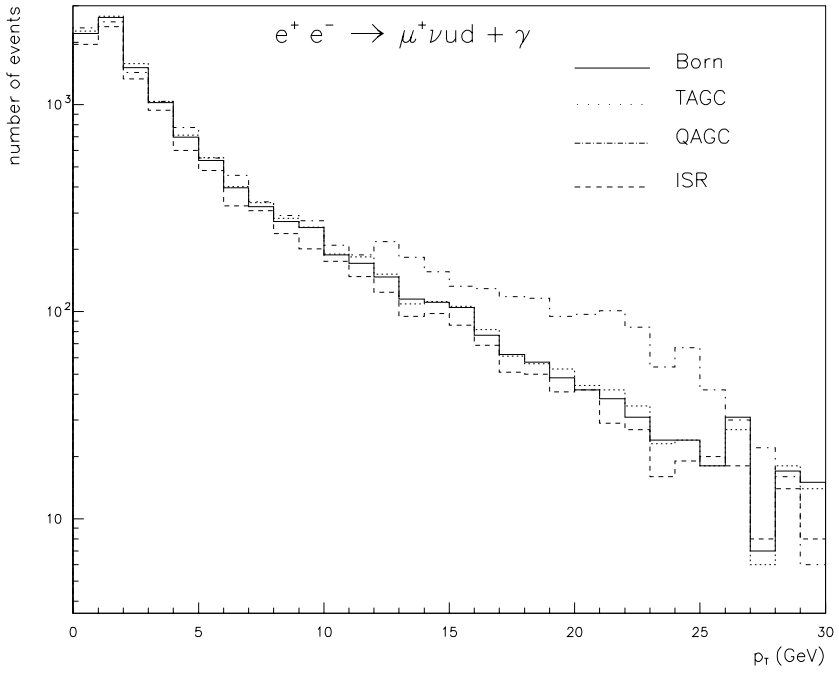

Fig. 13. The distribution of the transverse momentum of the visible photon for the process $e^+e^- \to \mu^+\nu_\mu\bar{u}d\gamma$ at $s^{1/2} = 192\,\mathrm{GeV}$. The event samples are the same as those of Fig. 10

sensitive to the separation angle $\vartheta_{\gamma\text{-}f}$ between photon and charged fermions, ranging from about 2% for $\vartheta_{\gamma\text{-}f} = 5°$ to about 7% for $\vartheta_{\gamma\text{-}f} = 1°$. For the realistic situation of a vanishing separation angle $\vartheta_{\gamma\text{-}\mu}$ a massive calculation is strictly unavoidable.

Particular attention has been devoted to the inclusion of ISR, as a consequence of the presence of an observed photon in the final state. The contribution of ISR has been studied in terms of collinear and $p_\perp$-dependent SF. Numerical results illustrate that ISR introduces corrections of the order of 10–15% on the integrated cross section. However, in order to get a reliable estimate of ISR corrections and to avoid double counting, $p_\perp$ photon effects have to be considered. It has been shown that the double counting, affecting the QED corrected cross section via collinear SF, may reach the 5% level in a realistic event selection and hence it has to be taken into account carefully. A more accurate evaluation of double-counting effects should however consider also the photonic radiation off final state charged fermions.

Both trilinear and genuinely quartic anomalous gauge couplings have been implemented in WRAP, and their effects on total cross section as well as on photon distributions have been investigated. The impact of TAGC on

the considered observables does not seem to be very sensitive to the cuts imposed on the detected photon, suggesting that W radiation is not easily disentangled from the fermion radiation. Thus $4f+\gamma$ final states are not the ideal place where to look for TAGC, if compared with $4f$ final states, which benefit of a higher statistics. On the contrary, these radiative processes are significantly affected by QAGC. In particular it has been shown that a difference in the effect of QAGC is present between the predictions of the complete calculations by means of WRAP and the ones obtained in the limit of on-shell W bosons, which is the approximation presently used in the literature. A more complete investigation of QAGC in radiative events at e^+e^- colliders is currently in progress.

Acknowledgements. The authors wish to thank F. Cavallari, D.G. Charlton, A. Denner, S. Dittmaier, M. Musy, C.G. Papadopoulos, M. Roth, D. Wackeroth, and the participants in the CERN LEP2 Monte Carlo Workshop for useful discussions. Particular thanks go to the authors of RacoonWW for the very helpful collaboration in numerical comparisons and to P. Bell, D.G. Charlton and M. Thomson for useful information and help concerning QAGC.

References

1. Physics at LEP2, edited by G. Altarelli, T. Sjöstrand, F. Zwirner, CERN 96-01, CERN, Geneva, 1996
2. Four-Fermion Production in Electron–Positron Collisions, M. Grünewald, G. Passarino et al., in Reports of the working groups on precision calculations for LEP2 Physics, edited by S. Jadach, G. Passarino, R. Pittau, CERN 2000-009, CERN, Geneva, 2000, hep-ph/0005309
3. M. Acciarri et al., Phys. Lett. B **490**, 187 (2000)
4. G. Abbiendi et al., Phys. Lett. B **471**, 293 (1999)
5. S. Spagnolo, Measurement of Quartic Gauge Boson Couplings at LEP, talk given at XXX International Conference on High Energy Physics, July 27–August 2, 2000, Osaka, Japan
6. J. Fujimoto et al., Nucl. Phys. Proc. Suppl. B **37**, 169 (1994)
7. F. Caravaglios, M. Moretti, Z. Phys. C **74**, 291 (1997)
8. T. Ishikawa et al., KEK Report 92-19, 1993; H. Tanaka, T. Kaneko, Y. Shimizu, Comput. Phys. Commun. **64**, 149 (1991); H. Tanaka, Comput. Phys. Commun. **58**, 153 (1990)
9. F. Caravaglios, M. Moretti, Phys. Lett. B **358**, 332 (1995)
10. A. Denner, S. Dittmaier, M. Roth, D. Wackeroth, Nucl. Phys. B **560**, 33 (1999); M. Roth, Precise Predictions for Four Fermion Production in Electron-Positron Annihilation, dissertation ETH Zürich No. 13363, 1999, hep-ph/0008033
11. S. Dittmaier, Phys. Rev. D **59**, 016007 (1999)
12. A. Pukhov et al., hep-ph/9908288; E.E. Boos et al., hep-ph/9503280
13. J. Fujimoto et al., Comput. Phys. Commun. **100**, 128 (1997)
14. A. Kanaki, C.G. Papadopoulos, Comput. Phys. Commun. **132**, 306 (2000)
15. F. Jegerlehner, K. Kolodziej, Eur. Phys. J. C **12**, 77 (2000)
16. F. Jegerlehner, K. Kolodziej, Fermion mass effects in $e^+e^- \to 4f$ and $e^+e^- \to 4f\gamma$ with cuts, hep-ph/0012250
17. See, for example, A. Dobado, A. Gómez-Nicola, A.L. Maroto, J.R. Pelaez, Effective Lagrangians for the standard model (Springer, 1997), and references therein
18. J.W. Stirling, A. Werthenbach, Eur. Phys. J. C **14**, 103 (2000)
19. G. Belanger et al., Eur. Phys. J. C **13**, 283 (2000)
20. J.W. Stirling, A. Werthenbach, Phys. Lett. B **466**, 369 (1999)
21. G. Belanger, F. Boudjema, Phys. Lett. B **288**, 201 (1992); Phys. Lett. B **288**, 210 (1992)
22. O.J.P. Eboli, M.C. Gonzalez-Garcia, S.F. Novaes, Nucl. Phys. B **411**, 381 (1994); G. Abu Leil, J.W. Stirling, J. Phys. G **21**, 517 (1995)
23. F. James, Rep. Prog. Phys. **43**, 1145 (1980)
24. U. Baur, D. Zeppenfeld, Phys. Rev. Lett., **75**, 1002 (1995); C.G. Papadopoulos, Phys. Lett. B **352**, 144 (1995); E.N. Argyres et al., Phys. Lett. B **358**, 339 (1995); W. Beenakker et al., Nucl. Phys. B **500**, 255 (1997); M. Beuthe, R. Gonzalez Felipe, G. Lopez Castro, J. Pestieau, Nucl. Phys. **B498** (1997) 55
25. M. Moretti, Nucl. Phys. Proc. Suppl. **89**, 190 (2000)
26. K. Gaemers, G. Gounaris, Z. Phys. C **1**, 259 (1979); K. Hagiwara, R.D. Peccei, D. Zeppenfeld, K. Hikasa, Nucl. Phys. B **282**, 253 (1987)
27. M. Bilenky, J.L. Kneur, F.M. Renard, D. Schildknecht, Nucl. Phys. B **409**, 22 (1993); **419**, 240 (1994)
28. S. Jezequel, Charged Triple Gauge Couplings at LEP, talk given at XXX International Conference on High Energy Physics, July 27–August 2, 2000, Osaka, Japan
29. G. Gounaris, J.L. Kneur, D. Zeppenfeld et al., Triple Gauge Boson Couplings, in [1], Vol. 1, p. 525
30. G. Gounaris, J. Layssac, F.M. Renard, Phys. Rev. D **61**, 073013 (2000)
31. See, for example, C. Matteuzzi, Measurement of Neutral Triple Gauge Boson Couplings at LEP2, talk given at XXX International Conference on High Energy Physics, July 27–August 2, 2000, Osaka, Japan
32. M. Acciarri et al., hep-ex/0102024; M. Acciarri et al., Phys. Lett. B **478**, 39 (2000); M. Acciarri et al., Phys. Lett. B **489**, 55 (2000)
33. F. Gangemi, Anomalous quartic couplings in six-fermion processes at the Linear Collider, hep-ph/0002142
34. G. Montagna, O. Nicrosini, F. Piccinini, Comput. Phys. Commun. **98**, 206 (1996)
35. G. Montagna, M. Moretti, O. Nicrosini, F. Piccinini, Nucl. Phys. B **541**, 31 (1999)
36. E.A. Kuraev, V.S. Fadin, Sov. J. Nucl. Phys. **41**, 466 (1985); G. Altarelli, G. Martinelli, in Physics at LEP, edited by J. Ellis, R. Peccei, CERN 86-02, CERN, Geneva, 1986, Vol. 1, p. 47; O. Nicrosini, L. Trentadue, Phys. Lett. B **196**, 551 (1987); Z. Phys. C **39**, 479 (1988); F.A. Berends, G. Burgers, W.L. van Neerven, Nucl. Phys. B **297**, 429 (1988)
37. C.M. Carloni Calame et al., Nucl. Phys. B **584**, 459 (2000)
38. G. Montagna, O. Nicrosini, F. Piccinini, Comput. Phys. Commun. **90**, 141 (1995); D.G. Charlton, G. Montagna, O. Nicrosini, F. Piccinini, Comput. Phys. Commun. **99**, 355 (1997)